Design and optimization of a hydrodynamically activated removable protective nose cover for high-speed water-entry vehicles

Tang Xuan Long*, Phan The Son

Institute of Missile, Academy of Military Science and Technology, 17 Hoang Sam, Nghia Do, Hanoi, Vietnam.

*Corresponding author: longtank2012@gmail.com

Received 04 Jun. 2026; Revised 18 Aug. 2026; Accepted 04 Sep. 2026; Published 16 Sep. 2026.

DOI: https://doi.org/10.54939/1859-1043.j.mst.FMC.2026.108-116

ABSTRACT

High-speed water entry subjects nose-mounted instrumentation of submersible vehicles, such as torpedoes and oceanographic instruments, to severe hydrodynamic impact loads. Conventional frangible nose covers often exhibit unreliable separation due to material property variations under environmental conditions. This paper presents a novel removable protective nose cover activated purely by hydrodynamic forces. The design consists of shell segments secured by a central nose member and attachment clips; submerged inlet ducts direct water into a trap groove beneath each clip, generating a pressure differential that triggers release. Using Sequential Quadratic Programming (SQP), key geometric and mechanical parameters were optimized to ensure reliable activation at a water-entry velocity of 90 km/h, with a high safety margin against premature release at transonic air speeds. Compared with conventional frangible covers, the proposed design offers greater reliability, repeatability, and environmental insensitivity, providing theoretical formulations and practical guidelines for hydrodynamic release mechanisms in aerospace and marine applications.

Keywords: Removable nose cover; Hydrodynamic release mechanism; High-speed water entry; Pressure differential activation; Water-trap groove.

1. INTRODUCTION

High-speed water entry of aerial-launched submersible vehicles, such as torpedoes, sonobuoys, and oceanographic instruments, is one of the most critical and structurally demanding phases in marine vehicle deployment [1, 2]. At impact velocities typically ranging from 50 to 100 km/h, the nose section experiences severe hydrodynamic slamming loads, high-pressure spikes, and cavitation phenomena that can damage sensitive acoustic arrays, sensors, and electronic components [3, 4].

To mitigate these impact forces, protective nose covers have been widely adopted to streamline the forebody and attenuate peak deceleration during water entry. The most common traditional solutions rely on frangible nose covers fabricated from specially engineered plastics or ceramics, designed to fracture or disintegrate upon water impact [5, 6]. However, these passive designs have major limitations: fracture strength is highly sensitive to environmental variables such as temperature, humidity, material aging, manufacturing defects, and impact angle [7, 8]. As a result, frangible covers frequently suffer premature fragmentation during transport, bird strikes, or flight vibrations, or fail to detach completely after water entry, obstructing sensors and compromising mission success [9, 10].

To overcome these drawbacks, research has shifted toward active detachment mechanisms. A significant contribution in this direction is the hydrodynamic release concept proposed by Kimerer et al. (2012) in U.S. Patent US 8,093,487 B2 [11]. The release mechanism is based on a pressure differential generated when water flows through submerged inlet ducts into water-trap grooves beneath the clips.

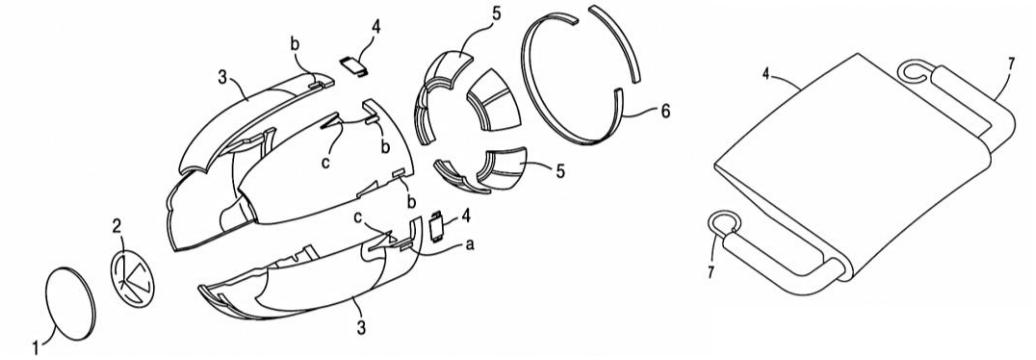


Figure 1. *Exploded view of the hydrodynamically activated removable protective nose cover (1- Central nose member; 2. Central nose foam cushion; 3. Protective shell member; 4. Attachment clip; 5. Shell foam insert; 6. Sealing gasket; 7. Torsional spring (wire); a. First clip slot; b. Second clip slot; c. Water-trap groove).*

Although the patented concept offers improved reliability and reduced dependence on material fracture properties, it provides limited quantitative analysis and engineering design guidelines for practical implementation. Previous studies on water entry dynamics [1, 2, 12] and hydrodynamic loading [3, 13] also lack detailed investigation into velocity-threshold release mechanisms using torsional elements.

Building upon the foundational patent, the present study develops a detailed analytical model and optimization of the hydrodynamic release mechanism. The primary objective is to optimize key geometric and mechanical parameters - particularly the water-trap groove width (b), depth (h), inclination angle (α), torsional wire properties, and moment arms - to achieve reliable activation at a target water-entry velocity of 90 km/h, while ensuring a high safety margin against premature release during high-speed airborne flight, including transonic conditions.

This paper presents the system architecture, the mathematical model of pressure differential and clip dynamics, the optimization methodology, results, and design recommendations.

2. METHODOLOGY

2.1. Computational model

Figure 2 illustrates the mechanical model utilized to evaluate the structural parameters of the interlocking attachment clip.

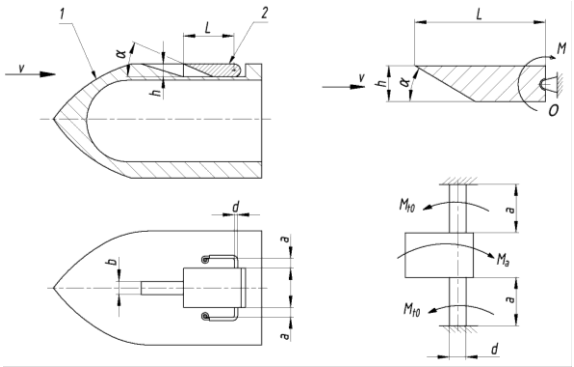


Figure 2. *Schematic diagram of the overall attachment clip and the torsion bar assembly (1 - Aerodynamic nose cone; 2 - Attachment clip; b - Water-trap groove width; h - Catching wedge depth; α - Surface inclination angle; L - Effective clip length; a - Effective torsion bar length; d - Torsional wire diameter; M_a - Aerodynamic opening moment; M_{t0} - Restoring moment of torsional bars).*

The interlocking attachment clip (hereinafter, the "attachment clip") is integrated into the aerodynamic nose cone shell [11], experiencing external aerodynamic/hydrodynamic freestream loading at velocity V and an elastic restoring torque delivered by the torsion bar system. The structural design space is defined by the effective attachment clip length L, the water-trap groove width b, and the catching wedge depth h. The external boundary of the attachment clip features a catching wedge profile inclined at an angle α relative to the nose cone moldline.

To establish an analytical model governing the mechanical deployment and locking transitions of the attachment clip about its center of rotation O, the following assumptions are introduced:

- The external freestream surrounding the nose cone is assumed to be continuous and incompressible within the investigated subsonic velocity regime [14].

- The attachment clip is treated as a perfectly rigid body rotating about a fixed, frictionless pin-joint at the pivot axis O.

The inclination angle α and the catching wedge depth h are decoupled as independent non-linear variables, avoiding small-angle approximations to preserve model fidelity.

2.2. Aerodynamic/hydrodynamic model and opening moment (M_a)

As the freestream fluid at velocity V flows over the nose cone, the inclined surface of the attachment clip acts as a flow-deflecting wedge [14], inducing an asymmetric pressure distribution across the 3D wedge geometry [3, 14].

The aerodynamic/hydrodynamic normal force (F_N) exerted perpendicular to the actual wetted surface area of the inclined wedge (S= $b \cdot h/\sin\alpha$) is formulated as:

$$F_N = C_N \cdot \left(\frac{1}{2}\rho V^2\right) \cdot \left(\frac{b \cdot h}{\sin\alpha}\right) \quad (1)$$

where ρ represents the freestream fluid density (kg/m^3) and V denotes the relative flow velocity (m/s).

The normal force coefficient C_N is inherently a non-linear function governed by the structural inclination angle α and the spatial boundary constraints of the water-trap groove (b, h). To account for local spanwise flow spillage across the lateral boundaries of the attachment clip (3D tip vortex losses), the coefficient C_N is generalized via a semi-empirical correction formula adapted from boundary-layer aspect-ratio and finite-span wing theories [3, 14]:

$$C_N = C_{N0}(\alpha) \cdot \left(1 - e^{-k \cdot \frac{b}{h}}\right) \quad (2)$$

Where $C_{N0}(\alpha)$ is the theoretical two-dimensional (2D) normal force coefficient defined as $C_{N0}(\alpha) = 2\pi \sin\alpha$ [14], the exponential term characterizes the force attenuation from lateral fluid bypass, and k is a dimensionless empirical calibration factor dependent upon the boundary conditions of the groove channel [14]. Generally, the value of k ranges from 0.5 to 2.0, varying with the structural configuration of the water-trap groove.

To isolate the net opening moment (M_a) acting about the trailing pivot axis O, the normal force F_N is projected onto the vertical axis normal to the attachment clip body using the geometric coefficient $\cos\alpha$. The distance from the center of pressure (defined at the midpoint of the horizontal projection of the wedge) to the pivot axis O yields the exact analytical moment arm:

$$d_{ad} = L - \frac{h}{2\tan\alpha} \quad (3)$$

By multiplying the vertically projected force component by the physical moment arm, the generalized non-linear opening moment equation is established:

$$M_a = (F_N \cdot \cos\alpha) \cdot d_{ad} \quad (4)$$

Substituting Equation (1) into Equation (4), the definitive expression for the opening moment

is explicitly derived in terms of independent geometric parameters, eliminating empirical aspect-ratio dependencies associated with conventional finite-span wing theories:

$$M_a(\alpha, V) = C_N \cdot \left(\frac{1}{2}\rho V^2\right) \cdot b \cdot h \cdot \cot\alpha \cdot \left(L - \frac{h}{2\tan\alpha}\right) \tag{5}$$

2.3. Torsion bar model and elastic restoring torque (M_{t0})

The retention and resetting mechanism of the attachment clip comprises two symmetric torsion bar strands [11], each with an effective torsional length *a* and a wire diameter *d*.

In the fully closed state ($\theta = 0$), a mechanical pre-twist angle $\theta_0 = 1\pi/180$ rad (or 1°) is initially locked into the assembly during manufacturing to sustain the seating pressure and groove sealing integrity. The total initial elastic restoring torque (M_{t0}) opposing the structural deployment is derived via Hooke's law for pure torsion [15]:

$$M_{t0} = 2 \cdot M_{t1} = 2 \cdot \frac{G \cdot I_p \cdot \theta_0}{a} \tag{6}$$

Where G is the shear modulus of the torsional wire material, $G = 79$ GPa, and I_p is the polar moment of inertia of the circular wire cross-section, $I_p = \pi d^4/32$. Substituting I_p into the primary relation yields the explicit formulation for the elastic restoring moment:

$$M_{t0} = \frac{\pi \cdot G \cdot d^4 \cdot \theta_0}{16 \cdot a} \tag{7}$$

2.4. Threshold activation condition

The interlocking attachment clip initiates its deployment sequence and lifts off the nose cone skin line if and only if the fluid-driven opening moment overcomes the structural pre-load torque of the torsion bar system in its undeflected state ($\theta = 0$):

$$M_a(\alpha, V_w) \geq M_{t0}(0) \tag{8}$$

By mapping the explicit non-linear hydrodynamic torque (Equation 5) and the elastic restoring torque (Equation 7) onto the activation boundary condition, the governing threshold equation is expressed as:

$$C_N \cdot \left(\frac{1}{2}\rho_w V_{th}^2\right) \cdot b \cdot h \cdot \cot\alpha \cdot \left(L - \frac{h}{2\tan\alpha}\right) = \frac{\pi \cdot G \cdot d^4 \cdot \theta_0}{16 \cdot a} \tag{9}$$

Solving Equation (9) isolates the critical threshold velocity (V_{th}) required to trigger the attachment clip:

$$V_{th} = \sqrt{\frac{\pi \cdot G \cdot d^4 \cdot \theta_0}{8 \cdot C_N \cdot \rho_w \cdot a \cdot b \cdot h \cdot \cot\alpha \cdot \left(L - \frac{h}{2\tan\alpha}\right)}} \tag{10}$$

The analytical model established at this boundary layer provides a direct, closed-form mathematical correlation between the structural parameters (L, b, h, a, d), the manufacturing inclination angle (α), the material elastic constants (G, θ_0), and the freestream hydrodynamic conditions (V, ρ). This expression serves as the mathematical foundation for the multi-variable optimization framework.

2.5. Formulation of the constrained optimization problem

To resolve the structural configuration of the attachment clip - ensuring deterministic deployment under low-velocity aqueous submersion ($V_{th} = V_w = 25$ m/s (90 km/h)) while enforcing strict structural immobility against premature aerodynamic activation during high-velocity atmospheric cruise (up to transonic Mach 1 airflows, $V_a = 340$ m/s) - the design task is formulated as a non-linear constrained programming problem [15].

Unlike conventional optimization models that minimize torque residuals, the primary objective here is to minimize the spatial envelope of the flow-deflecting wedge, reducing aerodynamic drag and cross-sectional weight while ensuring compliance with multi-medium safety thresholds.

- Design Vector: The spatial configuration of the attachment clip is defined by a six-dimensional optimization vector comprising both geometric and mechanical variables: $\mathbf{X} = [b, h, \alpha, L, d, a]^T$

- Minimize Objective Function: The objective function isolates the projected cross-sectional area of the catching wedge profile, formulated as: Minimize $f(\mathbf{X}) = b \cdot h$

Design space constraints

The admissible boundaries for the geometric design variables, governed by manufacturing tolerances and envelope limitations, are defined as:

$$\Omega = \begin{cases} 10.0 \leq b \leq 20.0 & \text{(mm)} \\ 4.0 \leq h \leq 7.0 & \text{(mm)} \\ 5.0 \leq \alpha \leq 15.0 & \text{(deg)} \\ 55.0 \leq L \leq 65.0 & \text{(mm)} \\ 3.5 \leq d \leq 5.5 & \text{(mm)} \\ 8.0 \leq a \leq 20.0 & \text{(mm)} \end{cases} \tag{11}$$

Functional performance constraints

The optimization framework must satisfy a coupled system of non-linear inequalities representing critical safety boundaries [15]:

$$g_1(\mathbf{X}): SF_{wat}(\mathbf{X}) = \frac{M_{hyd}(\mathbf{X})}{M_{t0}(\mathbf{X})} \geq n_o \tag{12}$$

$$g_2(\mathbf{X}): SF_{aer}(\mathbf{X}) = \frac{M_{t0}(\mathbf{X})}{M_{aer}(\mathbf{X})} \geq n_c \tag{13}$$

Where:

- Constraint $g_1(\mathrm{X})$ dictates the prerequisite hydrodynamic deployment condition, ensuring the actual opening safety factor (SF_{wat}) under aqueous submersion matches or exceeds the target opening coefficient ($n_o = 1.5$). This indicates that the fluid driving moment (M_{hyd}) at $V_w = 25$ m/s overcomes the baseline material pre-load with a 50% energy reserve.

- Constraint $g_2(\mathrm{X})$ acts as the aerodynamic safety barrier, requiring that the actual closing safety factor (SF_{aer}) remains greater than or equal to the target retention coefficient ($n_c = 2.5$). This ensures that the mechanical pre-load torque (M_{t0}) delivered by the torsion bar assembly under a tight pre-twist angle ($\theta_0 = 1.0°$) maintains a minimum 150% structural energy reserve over the maximum aerodynamic disturbing moment (M_{aer}) at Mach 1 ($V_a = 340$ m/s). This prevents premature deployment triggered by transonic shockwave variations, atmospheric turbulence, or vehicle vibrations.

2.6. Non-linear global optimization scheme via evolutionary search method

The structural governing constraints (g_1, g_2) exhibit severe higher-order non-linearities and multi-dimensional geometric coupling within the defined design space Ω. Specifically, the wire diameter (d) introduces fourth-power scaling in the torsional loading formulations, which is coupled with the unapproximated trigonometric functions ($\cot\alpha$, $\tan\alpha$) governing the hydrodynamic center of pressure. Because the safety criteria (SF_{hyd}, SF_{aer}) establish opposing boundary requirements on the wedge dimensions, the resulting objective function topology is highly non-convex and characterized by a rugged response surface. Under these conditions, conventional gradient-based optimization algorithms are prone to premature stagnation at local minima [15].

To overcome this optimization challenge and achieve robust global convergence toward the minimum envelope, an evolutionary direct search framework is implemented [15, 16]. The solution routine utilizes the sequential quadratic programming (SQP) optimization suite within the Maple computational environment, combined with automated design space exploration.

The evolutionary optimization algorithm proceeds through the following phases [15]:

- Population initialization: The numerical solver randomly populates a diverse set of candidate design vectors $\mathbf{X}_i = [b, h, \alpha, L, d, a]^T \in \Omega$ across the design space, ensuring unbiased initial exploration [16].

- Fitness evaluation and penalty function handling: For each candidate vector $\mathbf{X}_i$, the objective value $f(\mathbf{X}_i) = b \cdot h$ is computed simultaneously with the functional inequalities. Infeasible design vectors that fail to provide sufficient underwater opening moment ($SF_{wat} < 1.5$) or violate the strict aerodynamic safety factor reserve ($SF_{aer} < 2.5$) are heavily penalized and excluded from the solution pool [15].

- Parameter space condensation: Bypassing localized gradient calculations, the algorithm iteratively subdivides the parameter bounding regions, driving successive candidate generations out of local valley traps toward the global optimum.

- Convergence criteria: The search terminates when the variance between successive candidate generations falls below a predefined tolerance ($\epsilon \leq 10^{-6}$), isolating the final nominal dimensions of the attachment clip, where the geometric footprint is minimized while all safety constraints remain satisfied.

3. RESULTS AND DISCUSSION

3.1. Optimization framework and convergence analysis

The non-linear programming problem for the pressure-sensitive attachment clip mechanism was solved within the Maple computational environment using the global evolutionary SQP routine. In this optimization cycle, the design objective was shifted from a localized torque residual minimization to a global geometric envelope reduction, specifically minimizing the projection area of the catching wedge ($b \cdot h$). The optimization process incorporated updated constraint vectors, including an opening safety factor ($n_o = 1.5$), a closing safety factor ($n_c = 2.5$), and an initial installation pre-twist angle ($\theta_0 = 1.0°$).

The evolutionary algorithm converged stably to the global minimum of the objective function:

$$\min f(\mathbf{X}) = b \cdot h = 0.473 \times 10^{-4}\ \text{m}^2$$

This minimized value represents the optimal bounding area of the fluid-deflecting wedge that sustains structural and functional integrity under multi-medium operation. The corresponding nominal dimensions extracted from the optimized design vector $\mathbf{X}_{opt}$ are detailed in Table 1.

Table 1. *Optimized nominal structural parameters of the attachment clip.*

Parameter	Symbol	Unit	Bound Range (Ω)	Optimized Value
Water-trap groove width	*b*	mm	10.0 - 20.0	**11.0**
Catching wedge depth	*h*	mm	4.0 - 7.0	**4.3**
Surface inclination angle	*α*	deg	5.0 - 15.0	**6.6**
Effective attachment clip length	*L*	mm	55.0 - 65.0	**61.0**
Torsional wire diameter	*d*	mm	3.5 - 5.5	**3.5**
Effective torsion bar length	*a*	mm	8.0 – 20.0	**15.8**

3.2. Quantitative evaluation of moment balance and safety margins

To validate the optimized configuration, the derived structural dimensions were back-substituted into the governing equations. The resulting system moments acting about the trailing pivot axis O are computed as follows:

- **Hydrodynamic opening moment (M_{hyd}):** 3.88 N · m (at $V_w = 25$ m/s in water)
- **Aerodynamic disturbing moment (M_{aer}):** 0.87 N · m (at $V_a = 340$ m/s in air)
- **Elastic restoring pre-load moment (M_{t0}):** 2.57 N · m (at $\theta_0 = 1.0°$)

These indicators reveal the mechanism's bi-stable operational behavior:

1. **Hydrodynamic responsiveness (opening safety margin):** The real-world opening safety factor under aqueous submersion achieves the exact target limit:

$$SF_{wat} = \frac{M_{hyd}}{M_{t0}} = 1.51 \quad (\geq n_o = 1.5)$$

   This numerical convergence indicates that the opening constraint is *active*. The optimized catching wedge features an expanded width ($b = 11$ mm) and an elevated inclination profile ($\alpha = 6.6°$) to aggressively harness the high density of water ($\rho_w = 1000$ kg/m^3). This generates a robust hydrodynamic normal force sufficient to overcome the torsion bar resistance with approximately 50% engineering safety backup, ensuring reliable detachment during water entry.

2. **Aerodynamic security (closing safety margin):** Concurrently, the structural locking integrity during high-speed airborne flight satisfies the safety requirement with a comfortable margin:

$$SF_{aer} = \frac{M_{t0}}{M_{aer}} = 2.94 \quad (\geq n_c = 2.5)$$

   The achieved aerodynamic safety factor of 2.94 is significantly higher than the designated minimum threshold of 2.5. This shows that despite the flattened pre-twist angle ($\theta_0 = 1.0°$) and water-trap groove width ($b = 11$ mm), the algorithm regulated the wedge depth to $h = 4.3$ mm and selected the minimum allowable wire diameter ($d = 3.5$ mm) coupled with an increased torsion bar length ($a = 15.8$ mm). This precise structural calibration limits the aerodynamic lift generation, providing a 194% mechanical energy reserve over the peak transonic air loads. Consequently, premature deployment from aerodynamic turbulence, shockwave interactions, or flight vibrations is effectively prevented.

3. **Geometric minimization logic:** The coupling between SF_{wat} and SF_{aer} highlights the effectiveness of the geometric minimization objective: the solver reduced the cross-sectional profile ($b \cdot h$) to its lowest functional limit without sacrificing airborne lockup or delaying hydrodynamic deployment.

4. CONCLUSIONS

This study has established a mathematical optimization framework for a hydrodynamically activated, removable protective nose cover. By implementing a non-linear constrained programming formulation solved via an evolutionary Sequential Quadratic Programming (sqp) routine, the conflict between high-speed airborne retention and low-velocity underwater deployment was resolved. The core conclusions are summarized as follows:

- **Mathematical validation of geometric minimization:** The optimization algorithm effectively minimized the projecting boundary area of the catching wedge to a global minimum of

0.473×10^{-4} m^2. This demonstrates that the wedge geometry can be scaled down to a compact envelope while maintaining torque equilibrium across both fluid media.

- Precision in hydrodynamic activation: Under the optimized configuration ($L = 61.0$ mm, $\alpha = 6.6°, b = 11.0$ mm, and $h = 4.3$ mm), the mechanism achieves an actual opening safety factor of $SF_{wat} = 1.51$, matching the design target ($n_o = 1.5$). This indicates that the clip will reliably lift off as the vehicle reaches the water-entry velocity threshold of 25 m/s.

- Robustness against premature airborne deployment: In the atmospheric flight regime up to transonic speed, Mach 1 (340 m/s), the system exhibits an actual closing safety factor of $SF_{aer} = 2.94$, comfortably exceeding the strict baseline requirement ($n_c = 2.5$). Even with a reduced pre-twist angle ($\theta_0 = 1°$), the optimized mechanical configuration provides a near-200% torque reserve, ensuring structural immobility against localized aerodynamic gusts, transonic shockwave pressure spikes, and vehicle vibrations prior to water impact.

- Engineering implementation guidelines: The optimized parameter interactions-utilizing the minimum wire diameter ($d = 3.5$ mm) and an increased torsion bar length ($a = 15.8$ mm) to balance a maximized width profile-offer generalized design rules, replacing traditional, climate-sensitive frangible covers with a repeatable, fluid-driven interlocking mechanism suitable for aerospace and marine vehicle applications.

In summary, this methodology provides a validated foundation for the design of pressure-sensitive interlocking release mechanisms operating under high-velocity, multi-medium flight profiles.

REFERENCES

[1]. T. V. Kármán, "*The impact on seaplane floats during landing*", NACA Technical Note No. 321, (1929).

[2]. C. M. Seddon and M. Moatamedi, "*Review of water entry with applications to aerospace structures*", International Journal of Impact Engineering, Vol. 32, No. 7, pp. 1045–1067, (2006).

[3]. O. M. Faltinsen, "*Sea Loads on Ships and Offshore Structures*", Cambridge University Press, (1993).

[4]. T. T. Truscott, B. P. Epps and A. H. Techet, "*Water entry of projectiles*", Annual Review of Fluid Mechanics, Vol. 46, pp. 355–378, (2014).

[5]. B. Guo, H. Liu and Y. Zhao, "*Experimental investigation on the water entry of frangible composite covers*", Ocean Engineering, Vol. 157, pp. 1–12, (2018).

[6]. Y. Li and X. Zhang, "*Material variability and reliability analysis of frangible nose caps*", Journal of Materials Engineering and Performance, Vol. 29, No. 4, pp. 2345–2356, (2020).

[7]. Z. Huang et al., "*Failure analysis of frangible radomes under high-speed water impact*", Composite Structures, Vol. 172, pp. 12–22, (2017).

[8]. J. Zhao et al., "*Environmental effects on the fracture behavior of ceramic frangible covers*", Ceramics International, Vol. 47, No. 12, pp. 16845–16853, (2021).

[9]. S. Kim and J. Park, "*Bird strike and handling damage assessment on protective nose covers*", Aerospace Science and Technology, Vol. 88, pp. 102–110, (2019).

[10]. R. W. Thompson, "*Reliability issues in frangible nose protection systems*", Naval Engineers Journal, Vol. 127, No. 3, pp. 45–53, (2015).

[11]. N. B. Kimerer et al., "*Removable protective nose cover*", U.S. Patent No. 8,093,487 B2, (2012).

[12]. A. May, "*Water entry and the cavity-running behavior of missiles*", Naval Ordnance Laboratory, (1975).

[13]. G. Yan et al., "*Hydrodynamic loading and cavity dynamics during high-speed water entry*", Physics of Fluids, Vol. 34, No. 5, p. 052101, (2022).

[14]. S. F. Hoerner, "*Fluid-Dynamic Drag: Practical Information on Aerodynamic Drag and Hydrodynamic Resistance*", Hoerner Fluid Dynamics, (1965).

[15]. S. S. Rao, "*Engineering Optimization: Theory and Practice*", 5th ed., John Wiley & Sons, (2019).

[16]. J. C. Helton and F. J. Davis, "*Latin hypercube sampling and the propagation of uncertainty*", Reliability Engineering & System Safety, Vol. 81, No. 1, pp. 23–69, (2003).

TÓM TẮT

Thiết kế và tối ưu hóa nắp bảo vệ mũi tách rời kích hoạt bằng thủy động lực học cho các phương tiện bay lao vào nước tốc độ cao

Việc lao vào nước ở tốc độ cao gây ra tải trọng va đập thủy động lực học rất lớn lên các thiết bị đo lường nhạy cảm được lắp ở mũi của các phương tiện ngầm, chẳng hạn như ngư lôi và thiết bị hải dương học. Các nắp chắn mũi dễ vỡ (frangible) truyền thống thường có hiện tượng tách rời không ổn định do sự biến đổi tính chất vật liệu dưới tác động của điều kiện môi trường. Bài báo này trình bày một thiết kế nắp bảo vệ mũi có thể tháo rời, hoạt động hoàn toàn dựa trên cơ chế kích hoạt thủy động lực học. Thiết kế bao gồm các phân đoạn vỏ được cố định bởi một chi tiết mũi trung tâm và các kẹp gắn; các rãnh dẫn nước khi ngập trong nước sẽ dẫn nước vào một rãnh bẫy (trap groove) bên dưới mỗi kẹp, tạo ra chênh lệch áp suất làm kích hoạt việc nhả kẹp. Bằng phương pháp Quy hoạch toàn phương liên tiếp (Sequential Quadratic Programming – SQP), các thông số hình học và cơ học then chốt đã được tối ưu hóa nhằm đảm bảo kích hoạt tin cậy tại vận tốc lao vào nước 90 km/h, đồng thời duy trì biên độ an toàn cao chống lại hiện tượng nhả sớm ở tốc độ bay cận âm trong không khí. So với các nắp chắn dễ vỡ truyền thống, thiết kế đề xuất mang lại độ tin cậy, khả năng lặp lại và tính ổn định trước điều kiện môi trường cao hơn, đồng thời cung cấp các công thức lý thuyết và hướng dẫn thực tiễn cho các cơ cấu nhả bằng thủy động lực học trong các ứng dụng hàng không vũ trụ và phương tiện hàng hải.

Từ khoá: Nắp mũi tách rời; Giải phóng thủy động lực học; Lao vào nước tốc độ cao; Chênh lệch áp suất; Rãnh bẫy nước.